IEEE Transactions on Industrial Electronics, vol. PP, pp. 1–1, 2023

Online Loss Calculation and Optimization of a M3C Driven Externally Excited SM

P. Bontemps, D. Biner, C. Münch-Alligne, *et al.*

POWER ELECTRONICS LABORATORY
ÉCOLE POLYTECHNIQUE FÉDÉRALE DE LAUSANNE

Online Loss Calculation and Optimization of a M3C Driven Externally Excited SM

Philippe Bontemps, *Student Member, IEEE*, Daniel Biner, *Student Member, IEEE,*
Cécile Münch-Alligné and Drazen Dujic, *Senior Member, IEEE*

***Abstract*—Pumped-hydro storage power plants are a truly renewable solution for large grid connected energy storage. The evolution towards variable speed operation increases their flexibility and efficiency and ensures their relevance on a changing energy market. Exploiting all possible degrees of freedom in the machine operation as to maximize efficiency of the overall system allows to increase the profitability of the plant. Doing so in real-time on the same hardware-in-the-loop platform used for the validation of the control algorithm saves time and resources. The results presented here are collected from a real-time hardware-in-the-loop platform containing an industrial control platform. This paper presents the most energy efficient steady-state and transient operation of an externally excited synchronous machine driven by a matrix modular multilevel converter for a pumped hydro storage power plant application. To this end this work presents a real-time compatible converter loss calculation applicable on the simplified implementation of the converter without need to model the individual switches.**

***Index Terms*—Hardware-in-the-Loop, Real-Time Simulations, Matrix Modular Multilevel Converter, Pumped Hydro Storage Power Plants, Variable Speed Drive, Optimal trajectory, Loss evaluation**

I. Introduction

THE ever increasing share of renewable energy sources such as PV panels and wind turbines, characterized by their stochastic energy production, requires large flexible grid connected storage. While Pumped Hydro Storage Power Plant (PHSP) constitute large grid connected storage, their conventional fixed speed operation lacks the required flexibility. The conversion to Variable Speed Drive (VSD), which leads to the required flexibility, is achieved through the addition of a Frequency Converter (FC) connected between the grid and the Synchronous Machine (SM). The additional degrees of freedom resulting from the variable speed operation such as SM stator and excitation currents, allow for a system efficiency optimization.

For externally excited SMs connected to a FC, the excitation current constitutes an additional degree of freedom that can be controlled as to achieve various goals. The FC decouples the SM from the grid and thus eliminates the requirement of the SM stator voltage to be adapted to the grid voltages. However, this additional degree of freedom is generally not optimized for given operating conditions. The system losses, which include the SM losses are depending on the current operating conditions, which is to be considered when computing the losses. This work explores the optimization of all degrees of freedom in machine control as to achieve the highest possible system efficiency.

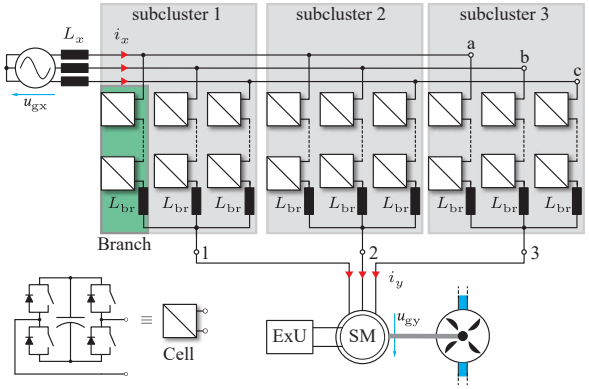

Fig. 1. The M3C with the three subclusters, highlighted in gray, each containing three branches, highlighted in green, and N cells per branch. The two AC systems connected to the terminals are represented by a grid on the input side and a 3 phase machine on the output side connected to a pump/turbine as is the case in a PHSP.

Extensive knowledge about the separate losses of the system are required as to allow an efficiency evaluation [1]. For large systems such as PHSP, the SM and FC are generally large custom made units produced in a small amount, and include extensive testing during which their characteristics are determined. Thanks to this knowledge, the system losses can be implemented in simulations prior to the deployment in the field and analysis regarding system efficiency can be done.

The converters such as the Matrix Modular Multilevel Converter (M3C), shown in Fig. 1, are able to offer the needed flexibility in the system design and optimization of the converter and machine voltage ratings of large PHSP by the series connection of cells [2]–[7]. However, this series connection of cells increases the complexity when it comes to the computation of the converter losses. Without any limitations on computational cost, a detailed calculation of all semiconductor losses can be done as presented in [8]. To avoid high simulation times, the relevant converter losses can be calculated by post-processing the relevant signals as presented in [9], [10]. While a computational cost effective method for the loss calculation of the MMC is presented in [11], it is valid only in steady-state and relies on the knowledge of the fundamental frequency of the branch current. Furthermore, due to the usage of Half Bridge (HB) cells, this method cannot be transferred to the M3C. Another method presented in [12], relies on the use of a virtual cell reducing the computational cost but still relying on post processing to extract the converter losses.

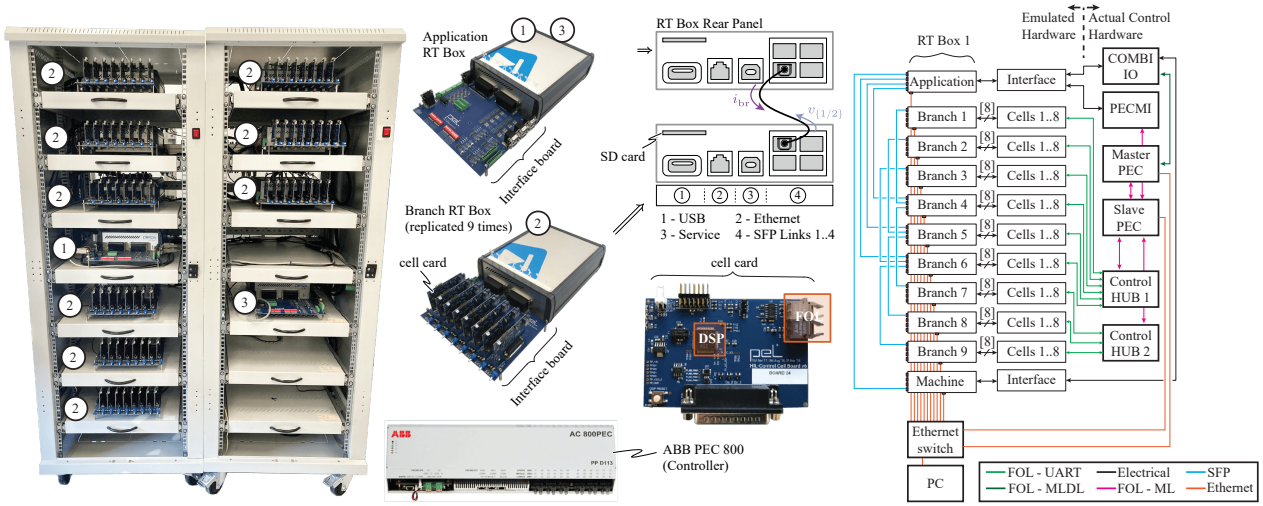

Fig. 2. Picture of the RT-HIL cabinet, including a schematic of the connection between the elements of the control structure. The 11 RT Boxes are hosting 3 different models: the grid side (number 1), the branches (number 2), and the machine model (number 3).

Prior to the deployment in the field, extensive testing including Real-Time (RT) Hardware-In-The-Loop (HIL) tests to validate the performance of the control algorithm are conducted. Generally these simulations disregard power losses of the system as their influence on the control algorithm is negligible. Additionally for complex systems such as the M3C computation limitations of RT computers may not allow the addition of the loss computation [13], [14]. This works extends the conventional usage of RT-HIL platforms, consisting of control validation, to include loss computation, thus allowing a RT optimization. Having the possibility of evaluating the overall system losses within the RT-HIL system enables optimization of system efficiency for transients and steady state operation. The RT-HIL platform used throughout this work is shown in **Fig. 2**.

The main contributions of this paper include the system level efficiency optimization of a PHSP as well as a RT compatible converter loss evaluation. Given the torque and speed references from a hydraulic Best Efficiency Point (BEP) tracking strategy during start-up in turbine mode [15], this work evaluates the overall system efficiency exploiting the machine flux as controllable degree of freedom. To achieve the efficiency optimization, a RT HIL compatible system loss calculation for the M3C using the sub-cycled average model is developed in this work. The calculation of the conduction and switching losses is done considering computational burden as to allow the implementation on small scale simulators such as the RT Box 1. Furthermore, compared to externally excited SM control optimization algorithms presented in various works [16], [17], this work requires neither a Finite Element Method (FEM) model of the SM nor does it require an online optimization problem solving routine to achieve optimal power loss as presented in [18].

This paper is organized as follows, section II presents the elements of the system to be optimized, section III covers the calculation of the switching and conduction losses of the sub-cycle average model of the M3C in real time. Section IV includes the measurement process on a 526 kVA SM for the evaluation of all the relevant losses including friction and ventilation as well as hysteresis and eddy current losses. Section V determines the optimal operating references for the SM reducing all the previously determined losses. Section VI demonstrates the power loss reduction for multiple operating regions and transients of a PHSP using the SM stator and excitation currents as a degree of freedom. Section VII concludes the work.

II. System Description

The system considered for the efficiency optimization is shown in Fig. 1. The converter, the M3C, is constituted of eight Full Bridge (FB) cells per branch with a nominal voltage of 1500 V. The characteristics of the cells correspond to the prototype in the ongoing development at the Power Electronics Laboratory (PEL) and can be found in the table I. The PQ diagram of the prototype is shown in **Fig. 3**. The per unit power corresponds to 500 kW. The simulated SM is a separately excited salient pole machine with an apparent power of 526 kVA and a nominal frequency of 25 Hz. The excitation of the SM is controlled through the ABB Unitrol 1020. As the hydraulic machinery is disregarded in this system optimization, the pump/turbine is modeled as an additional inertia on the machine shaft with a controlled torque output modeling the hydrodynamic load.

Prior to optimizing the efficiency of the overall system, the different losses of the various elements have to be defined. This includes M3C losses, machine losses as well as excitation system losses. The losses considered within the

TABLE I: Cell characteristics. Each cell requires four semiconductor devices and has 5 series and 4 parallel connected capacitors.

Capacitors	TDK B43630A5108M0	1000 µF, 450 V
Semiconductors	IXYS IXBF55N300	3000 V, 34 A
Cell nominal voltage	V_{cell}	1500 V
Switching Frequency	f_{sw}	1 kHz

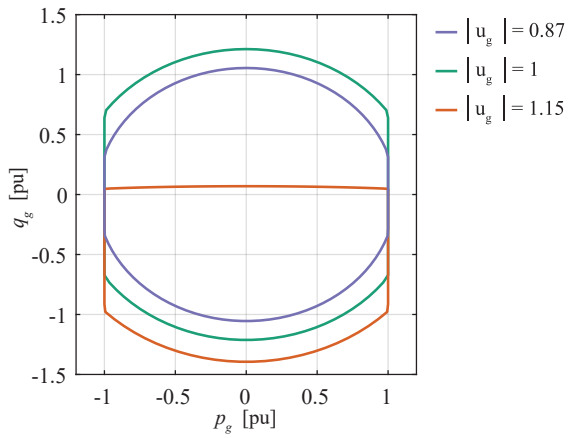

Fig. 3. PQ diagram of the M3C that is considered in this paper.

M3C include semiconductor conduction and switching losses as well as branch resistive losses and cell capacitor losses. The high amount of switches require special considerations when evaluating their losses as to maintain a low computational cost and allow RT simulations. For the SM the losses include stator and rotor conduction losses, friction and ventilation losses as well as eddy current and hysteresis losses. Additionally the losses of the excitation system are included in the calculation.

The evaluation of the here mentioned losses in RT can be achieved in three different ways. The first one being their offline evaluation and storage into lookup tables implemented in RT. While this method has a very low computational burden, it requires extensive offline simulations as to guarantee the validity of the lookup table for various operating points. The second method requires an offline evaluation as well as an identification of the entities influencing the losses which allows to determine the parameters of the function and implement this function in RT. The third method computes the losses in RT without prior offline evaluation. While this method generates the most reliable results, it requires the highest computational resources of all three methods. As will be elaborated in the following section, this work relies on both the second and third method for the converter and machine loss computations, respectively.

The system loss evaluation is done for a full load pumping operation as well as a start of the unit in turbine mode. The shaft speed and load torque references for the turbine start-up are generated taking into account hydraulic efficiency that also yields benefits in terms of fatigue damage to the mechanical system. Since more flexibility also implies more frequent start and stop cycles, stresses on the hydro-mechanical system during transient operations must carefully be studied. The synchronization phase required to couple fixed speed turbine units to the grid is known for its harmful hydrodynamic conditions. Thanks to the speed control possibilities enabled by the FC, soft starts can be realized by avoiding damaging operating ranges. Based on Computational Fluid Dynamics (CFD) simulations and structural Finite Element Analysis (FEA) performed by [15], a fixed speed turbine start-up sequence is compared to the variable speed start-up sequence with hydraulic BEP tracking strategy considered in this paper. In the latter case, important mitigation of fatigue damage of the hydraulic runner is predicted by the numerical models. Moreover, the duration of the start-up is drastically reduced that yields improvements regarding the Fast Frequency Response (FFR) capabilities of the PHSP.

III. Loss Calculation of the M3C using Sub-Cycle Averaged Model

The branch model used on the RT-HIL computers relies on the use of the sub-cycle average model as shown in Fig. 4. The description of which is given in [19] and the validity of the HIL platform using this modeling approach is shown in [13]. The advantage of the sub-cycle average model is the reduced amount of switches required to model a system such as the M3C. The reduced number of switches reduces proportionally the number of state spaces which allows for the use of small RT computers to model a complex system such as the M3C. However, by not modeling all the switches, the evaluation of the losses together with the requirement of low computational cost is more complicated. When using the HIL platform for control validation, the evaluation of the losses is often neglected as the objective lies in the verification of the control software and hardware. However the evaluation of the optimal operating point in RT requires a correct implementation of the converter loss calculation.

Fig. 4 illustrates the implementation of a branch of the M3C using the sub-cycle average model. The part highlighted in gray is vectorized, which means that the signals $S_1, S_2, S_3, S_4, v_1, v_2$ are vectors of dimension N. As we have eight cells per branch on the implemented M3C model, the dimension of the given vectors is eight, $N = 8$. As each branch is simulated using two controlled voltage sources, the elements of the vectors representing the cell voltages are to be summed up as to generate a non-vectorized value representing the equivalent branch voltage.

The computation of the losses from the available signals of Fig. 4 is divided into multiple stages. In the first stage, the inserted voltage of each cell within the branch is computed which is shown in Fig. 5. This has to be a vectorized entity as the variation in the cell capacitance voltage results in each cell having a different terminal voltage which needs to be determined.

In a second stage, depending on the respective cell voltage and the branch current direction, the number of diodes and

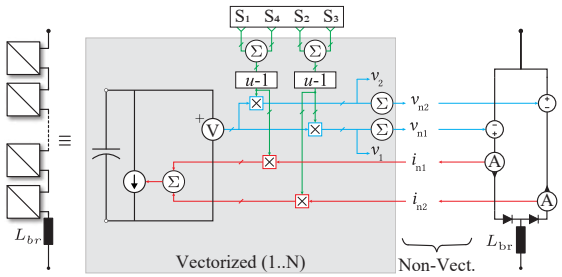

Fig. 4. Modeling of the M3C branch using the sub-cycle average model. The vectorized parts include eight elements as the simulated M3C has eight cells per branch.

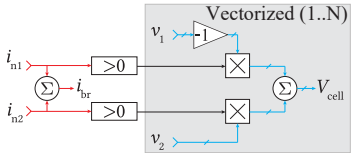

Fig. 5. Calculation of each individual cell terminal voltage based on the branch current and voltages from the sub-cycle averaged model.

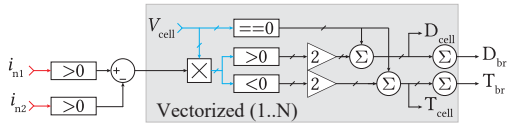

Fig. 6. With the direction of the branch current as well as the cell terminal voltage, the number of conducting diodes and Insulated Gate Bipolar Transistors (IGBTs) within a given branch at a given time instance is calculated.

transistors that are conducting is determined as shown in Fig. 6. The input signal i_{n1} is the positive branch current and remains zero whenever the branch current has a negative value. The signal i_{n2} shows the absolute value of the branch current in case of a negative branch current and remains zero whenever the branch current is positive. With these signals, a square signal of value $+1$ for a positive branch current and -1 for a negative branch current is generated. Whenever the cell terminal voltage multiplied by the previously mentioned square signal is positive, the given cell has two diodes conducting. On the other hand a negative product of both means that two transistors are conducting. When the cell terminal voltage is zero, independently of the branch current direction, the given cell has one switch and one diode conducting. The outputs D_{cell} and T_{cell} are vectors of dimension 8 with each element showing the number of diodes respective transistors that are conducting for that given cell. Summing up the elements of the vectors results in two non-vectorized values, D_{br} and T_{br} which represent the number of diodes and transistors that are conducting for a given branch.

The conduction losses are determined as shown in Fig. 7. Using two 2D-lookup tables with the temperature and the branch current as input, the on state voltage drop of the diode and the transistor is determined. These lookup tables are determined using data sheet values of the given diodes and transistors which usually give the on state voltage drop for two temperatures. The lookup table interpolates or extrapolates these values depending on the branch current and the

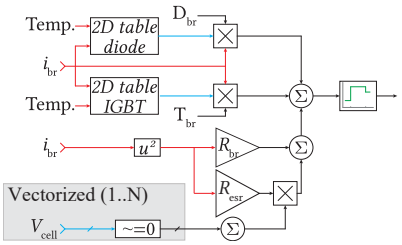

Fig. 7. Calculation of the conduction losses of each branch. The lookup tables provide forward voltages of diodes and IGBTs for the given temperature and branch current. Additionally the power loss in the branch resistance and in the cell capacitor is computed.

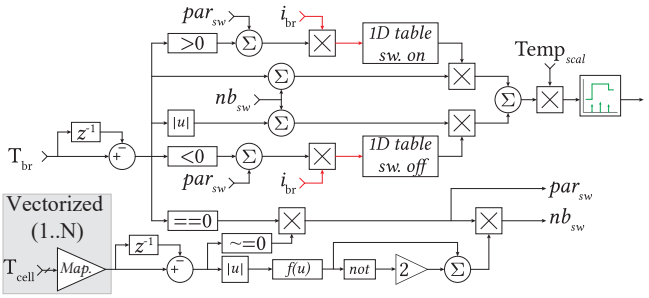

Fig. 8. Calculation of the M3C branch switching losses. Through the variation of the number of conducting IGBTs, the number of switching events is determined and the corresponding power loss is computed. The diode reverse recovery losses are included within the switch on lookup table of the IGBTs.

operating temperature. Finally simply multiplying the voltage drop with the branch current and the number of devices that are conducting results in the instantaneous branch conduction losses. Additionally, the losses through the branch resistance and cell capacitor are determined and added to the previously calculated conduction losses.

The computation of the switching losses is more challenging as shown in Fig. 8. The principle of this computation relies on the detection of a change in the number of transistors that are conducting within a given branch between two simulation time steps. A positive value indicates that not only a transistor turned on, but also a diode turned off, thus the reverse recovery losses should be considered. Similarly if the change is negative, this translates into a turn-off event of a transistor. Multiplying this change detection signals with the measured branch currents and feeding it into a lookup table results in the energy loss of the given switching action. However, as multiple switching events within a given branch can occur simultaneously, this energy is multiplied by the amplitude of the change of the number of conducting transistors which represents the number of transistors that switched at the given time instance. The temperature scaling of the losses is done using the equation $P_{\mathrm{sw}}(T) = P_{\mathrm{sw}}(T_0)\,(1 + K_T\,(T - T_0))$ as presented in [20].

While the description above results in a very good approximation of the losses, it fails to detect whenever two cells of the same branch turn transistors on and off simultaneously which results in a constant number of transistors conducting. The lower part of Fig. 8 detects these simultaneous switching events. The variable par_{sw} takes the value 1 whenever such an event occurs, and the nb_{sw} determines the number of transistors that switched simultaneous at that time instance. The vector T_{cell} includes one element with the number of transistors conducting for each cell. To reduce computational cost and not evaluate each element of the vector for a change, it is multiplied by a mapping vector which makes sure that any change in the initial T_{cell} results in a distinctive value after the multiplication with the mapping vector. Analyzing this distinctive value allows to determine if a simultaneous switching event occurred and how many switches are involved.

Fig. 9 illustrates the results of the loss calculation, taking as an example the first branch of the converter. At full

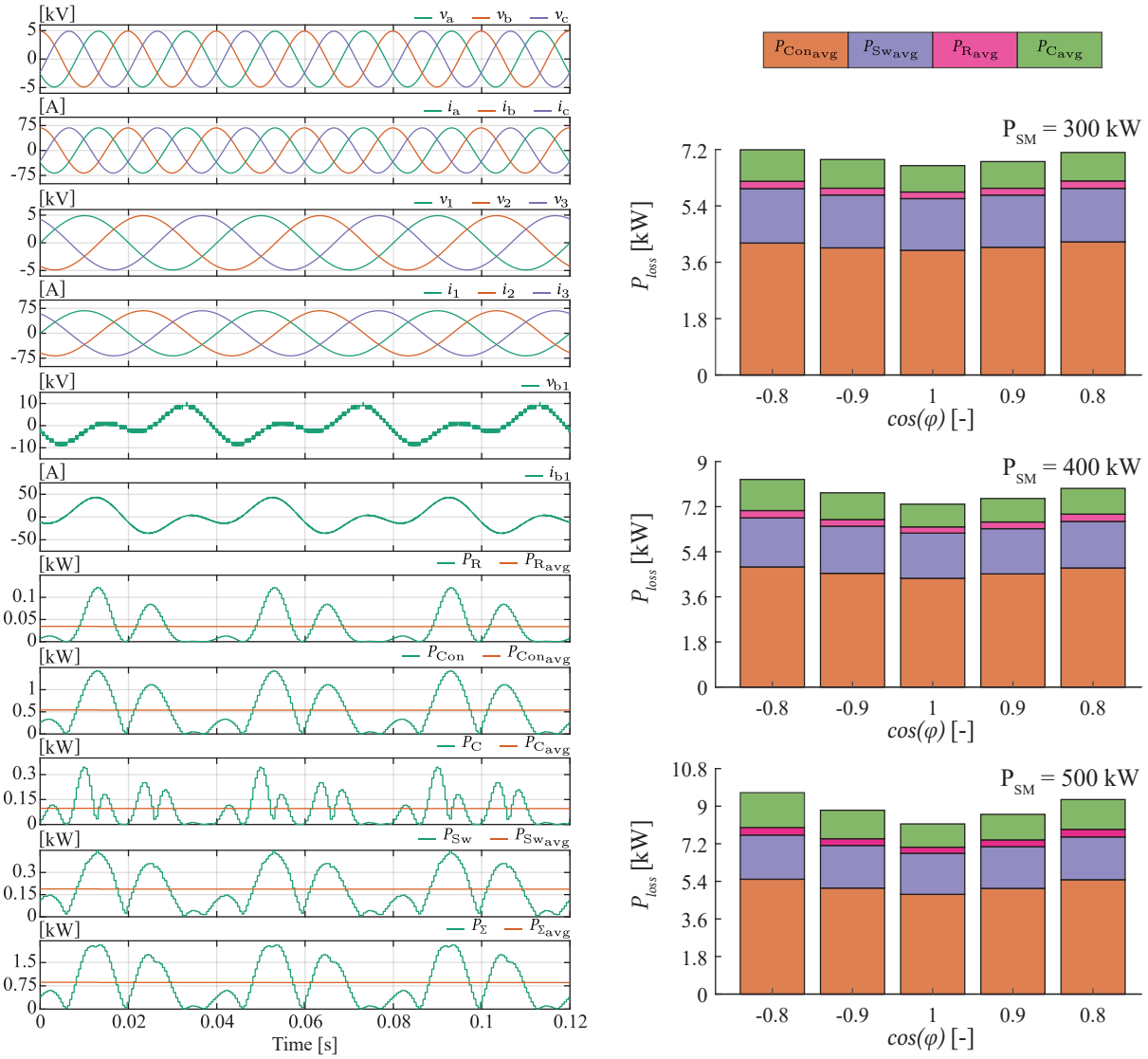

Fig. 9. Results of the introduced M3C loss calculation for an operating point at full power with a detailed illustration of all calculated losses in branch 1 shown on the left side. The right side shows the losses of the whole converter for various grid side power factors and for various active power references.

power operation, as shown in Fig. 9, the average loss through a branch is around 850 W. The following nomenclature is adopted for the various losses, P_{R} for the branch resistive losses, P_{C} for the cell capacitance losses, P_{Con} for the semiconductor conduction losses, P_{Sw} for the semiconductor switching losses including the reverse recovery losses of the diode. P_{Σ} is the sum of all branch losses. The capacitor losses are calculated based on the equivalent series resistance value extracted from the data sheet accounting for the dc link being made of 5 series and 4 parallel capacitances per cell. The final expression of the losses is: $P_{\mathrm{C}}(t) = i_{\mathrm{C}}^2(t) R_{\mathrm{esr_{eq}}}$. For the given operating point, the semiconductor conduction losses represent the highest losses in the overall branch losses with an average of 540 W, followed by the switching losses with 190 W. The relatively low switching losses are caused by the low switching frequency of the individual cell. The capacitor losses average 90 W and the branch resistive losses account for 30 W. The overall average converter losses at this operating point are at 7.6 kW resulting an efficiency of 98.5%.

IV. Synchronous Machine Loss Determination and Implementation

Additionally to the M3C switching and conduction losses, the SM is a major source of losses in the system. Four types of losses are characterized and simulated in this work. Firstly the stator and rotor winding losses $P_{\mathrm{S_L}}$, defined by the respective resistance and the instantaneous current measurement. Secondly the friction and ventilation losses $P_{\mathrm{fv_L}}$, which are dependent on the mechanical rotational speed of the machine. On the other hand there are the hysteresis and the eddy current losses $P_{\mathrm{HE_L}}$, which are dependent not only on the rotational speed of the machine but also on the magnetic flux.

In addition to the SM losses, the losses from the excitation converter have to be determined. The excitation unit, the ABB Unitrol 1020, controls the magnetic flux through the SM by controlling the excitation current. Through measurements,

TABLE II: SM ratings.

Apparent power	S	526 kVA
Power	P	500 kW
Stator voltage	V_s	6.3 kV
Stator current	I_s	53 A
Excitation. current (max)	I_exc	8.8 A (16 A)
Torque	T_m	3044 Nm
Speed	n	1500 rpm
Inertia	J	11.2 kg m^2

the losses of the Unitrol 1020, presented in **Fig. 10**, are determined. These losses are implemented as lookup table on the RT-HIL platform.

The estimation of the stator winding losses in the RT simulation is straight forward using the stator current amplitude calculated from the amplitude invariant Park transformation. With the data sheet value of the stator resistance and the previously calculated stator currents, the power losses can be calculated. A similar approach is used to determine the rotor winding losses.

The evaluation of the other SM losses requires either a FEM analysis or experimental measurements on the given SM, together with the angular momentum laws (1)-(2) [21].

$$\mathrm{M}\big|_{\psi_m} = \mathrm{J}\frac{d\omega_\mathrm{m}}{d\mathrm{t}}\bigg|_{\psi_m} \tag{1}$$

$$\mathrm{P}\big|_{\psi_m} = \omega_\mathrm{m}\mathrm{M}\big|_{\psi_m} \tag{2}$$

Where J is the machine inertia, ω_m the mechanical rotational speed in $^{rad}/_{s}$, M is the mechanical torque produced on the shaft and P the mechanical power. With the knowledge of the shaft total shaft inertia, and the measurement of the speed variation, the mechanical torque can be determined using (1). As both $P_{\mathrm{fv_L}}$ and $P_{\mathrm{he_L}}$ result in frictional torque acting on the shaft, evaluating this torque while controlling the magnetizing flux ψ_m to a known value, allows to determine these losses.

The SM that is characterized in this work is shaft connected to an IM as seen in **Fig. 11**. For this deceleration measurements, the IM is driving the SM which has open stator windings and the ABB Unitrol 1020 excitation system controlling the excitation current. The parameters of the SM are given in table II.

The results from the deceleration measurement is shown in Fig. 12. The excitation current was increased from 0% to 100% of its maximum value in steps of 10%. A total of 12

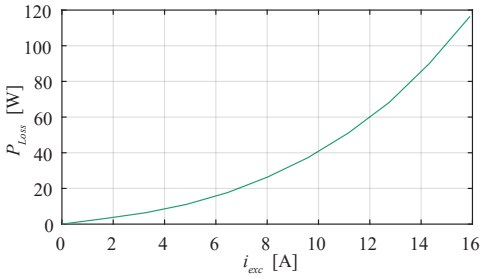

Fig. 10. Measured power losses of the excitation system (Unitrol 1020) over the full excitation current range.

Fig. 11. Picture of the Medium Voltage (MV) test bench, in dark blue the SM and in light blue the Induction Machine (IM). Both machines are rated at 500 kW and are connected on the same shaft.

measurements are conducted, with two measurements done without any excitation current. The reason for the repetition of the first measurement at the end is to evaluate the influence of changing machine conditions throughout the measurement process, i.e. temperature. As expected and can be observed on Fig. 12, the higher the excitation current, the faster the deceleration translating into a higher breaking torque due to the increased losses.

The frictional losses are varying linearly with the rotational speed, whereas the ventilation losses have a cubic relation with the speed. With this knowledge, one can create a function including a friction parameter (k_f), a ventillation parameter (k_v) and $w_{nom} = 1500\frac{\pi}{30}$.

$$P_{\mathrm{fv_L}} = k_v\left(\frac{w_m}{w_{nom}}\right)^3 + k_f\left(\frac{w_m}{w_{nom}}\right) \tag{3}$$

The test measurement done without any excitation current allow for the calculation of the torque and power losses generated by the friction and ventilation losses using (1) and (2). The inertia used in the calculation should correspond to the sum of the SM and IM inertias. Using the power losses from the measurement the parameters k_f and k_v from (3) can be derived to match the equation to the SM parameters. However, during the measurements, both machines, the IM as well as the SM are connected to the shaft, thus the measurement represent the sum of the frictional and ventilation losses of both the machines. As both machine have similar dimensions,

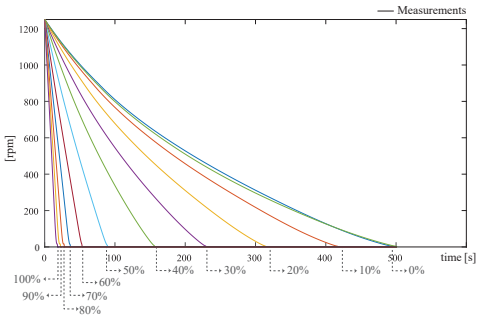

Fig. 12. Measurement result of the deceleration measurement of the SM under varying excitation current.

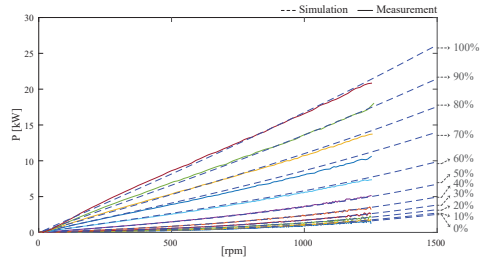

Fig. 13. Illustration of the measured power losses due to eddy currents and hysteresis and comparison to the simulation losses depicted with dotted lines. The comparison covers the whole range of excitations currents in steps of 10%.

the assumption of equal power loss can be made, thus half of the measured losses are occurring in the SM.

Before extracting the hysteresis and eddy current losses, the influence of the friction and ventilation losses need to be eliminated from the measurements. Similar to the frictional and ventilation losses, an equation representing the variation of the hysteresis and eddy current losses is required for the simulation [1]. This equation includes a hysteresis parameter (k_h) and an eddy current parameter (k_e) which are both expressed as a function of the magnetizing flux.

$$P_{\mathrm{he_L}} = k_h(\psi_m)\left(\frac{w_m}{w_{nom}}\right) + k_e(\psi_m)\left(\frac{w_m}{w_{nom}}\right)^2 \tag{4}$$

Fig. 13 illustrates the good match between measurements and simulation using the power loss expression described above for various excitation currents.

Using the per unit system, the measurement results from the 50 Hz SM presented above are rescaled to the 25 Hz SM modeled on the HIL.

V. Optimal Trajectory

The degrees of freedom that are used for the optimization include stator and excitation current of the SM. While additional efficiency optimization can be achieved by hardware modification of the FC such as the semiconductor choice or even considering a variation in switching frequency, this paper is based on the FB cell using unipolar modulation with a 1 kHz carrier frequency. For PHSP with a defined hydraulic head and a given power reference issued by the grid operator, speed and torque of the shaft are defined and cannot be used as a degree of freedom. In this optimization, the aim is to achieve the lowest losses within the electrical system by optimizing SM stator and rotor currents. The losses that are considered have been presented in the previous sections.

Analyzing the influence of each degree of freedom on the various losses offers an insight on their impact to reduce the overall system losses. While both direct and quadrature stator currents can be controlled individually, for a given direct and excitation current, the quadrature current has only a single value that fulfills the required shaft torque. For the SM with salient poles presented above, the mechanical torque can be expressed as:

$$\mathrm{M_{SM}} = \frac{3}{2}p\left(L_{\mathrm{md}}\big|_{i_m} i'_{\mathrm{ex}} i_{\mathrm{q}} + (L_{\mathrm{d}} - L_{\mathrm{q}})\big|_{i_m} i_{\mathrm{d}} i_{\mathrm{q}}\right) \tag{5}$$

The adapted approach for the modeling of the SM is the single saturation factor approach, introduced in [22], [23]. Where the saliency factor m is defined as a constant depending on the unsaturated main direct and quadrature inductances. With this approach, it is assumed that both d- and q-axis inductances saturate to the same level.

$$m = \frac{L_{\mathrm{mq0}}}{L_{\mathrm{md0}}} \tag{6}$$

Additionally using the isotropic equivalent model of the salient pole SM machine, a single magnetization flux as well as magnetization current can be defined:

$$\Psi_{\mathrm{m}} = \sqrt{\Psi_{\mathrm{md}}^2 + \frac{\Psi_{\mathrm{mq}}^2}{m}} \tag{7}$$

$$i_{\mathrm{md}} = i'_{\mathrm{ex}} + i_{\mathrm{d}} \quad \text{and} \quad i_{\mathrm{mq}} = i_{\mathrm{q}} \tag{8}$$

$$i_{\mathrm{m}} = \sqrt{i_{\mathrm{md}}^2 + m i_{\mathrm{mq}}^2} \tag{9}$$

When controlling the stator currents as to have the smallest possible value for the required torque, the P_{M3C} as well as the $P_{\mathrm{SM_{res}}}$ are minimized as these power losses are solely determined by the magnitude of the stator currents. However, no consideration is given to the hysteresis and eddy current losses $P_{\mathrm{he_L}}$. Thus this operating point might not correspond to the lowest overall losses. From (5), it is intuitive that the reluctance torque and thus also the highest torque per ampere is achieved with a positive d-current. However, the variation of the inductances due to the saturation cannot be neglected in (5). An increase in d-current leads to an increase in magnetizing current which in turn may lead to a decrease of the inductance, thus also a decrease in the produced torque.

Fig. 14 shows the best torque per amp operating point with and without saturation taken into account. Without saturation, the optimal d-current component will always be positive as this will result in a positive reluctance torque in (5). However, saturation created by the increase in d-current component leads to a reduction in the inductances L_{md} and L_{mq}. This influences not only the reluctance torque but reduces also the airgap torque, thus the optimal d-current can be negative as shown in Fig. 14.

The optimization routine implemented in Matlab that generates Fig. 14 includes all considered machine losses including resistive, friction and ventilation, hysteresis and eddy current

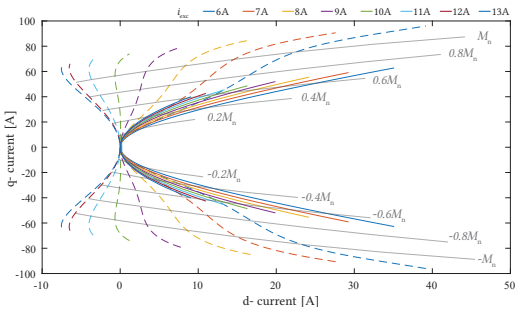

Fig. 14. Highest torque per ampere points for various excitation currents. The continuous lines indicate the result when neglecting the saturation effect and the dotted lines in the same color include saturation effects of the SM.

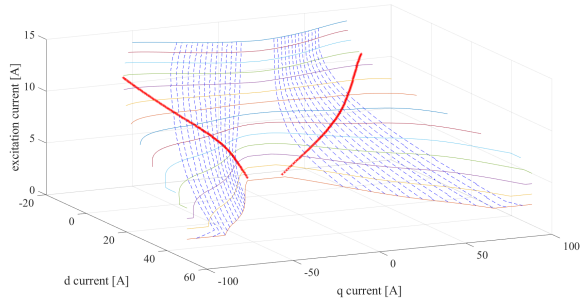

Fig. 15. Best torque per ampere operating points for various excitation currents. The blue dotted lines indicate the constant torque lines and the red dots indicate the optimal current references for a given torque.

losses. To create an optimization function including the exact semiconductor switching and conduction losses results is a very tedious task, as taking the example of the M3C, the branch current frequency and amplitude depends on the amplitudes and frequencies and phase shifts of the input and output ac system.

The mathematical expression of the optimization is presented below. The first constraint includes the SM torque presented in (5) and makes sure it fulfills the torque reference considering the frictional torque resulting from (3) and (4).

$$
\begin{aligned}
\underset{(i_\mathrm{d},i_\mathrm{q},i_\mathrm{e})}{minimize}: \quad & f\left(i_\mathrm{d},i_\mathrm{q},i_\mathrm{e}\right)=\frac{3}{2}\left(i_\mathrm{d}^2+i_\mathrm{q}^2\right)\mathrm{R_s}+i_\mathrm{e}^2\mathrm{R_r}\\
constraints: \quad & \mathrm{M_{SM}}=\mathrm{M^*}+\mathrm{M_{Loss}}\\
& \sqrt{i_\mathrm{d}^2+i_\mathrm{q}^2}<100\\
& |i_\mathrm{d}|<50\\
& i_\mathrm{e}<16
\end{aligned}
$$

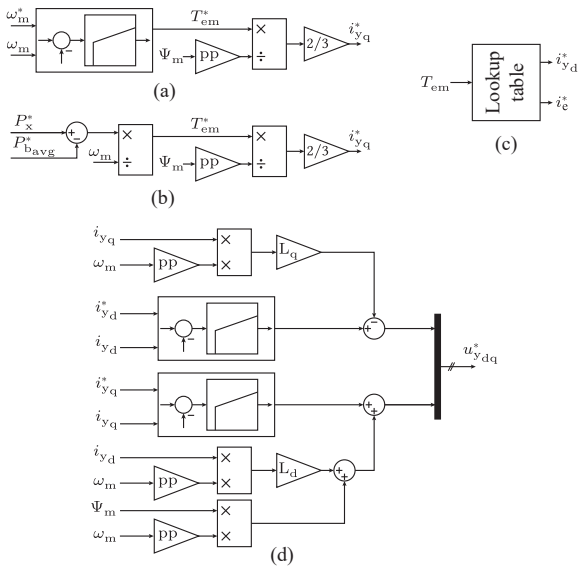

Fig. 16. Detailed view of the SM control structure. (a) showing the q-current reference computation when in speed control mode. (b) showing the q-current reference computation when in power mode, (c) showing the computation of the d-current and excitation current reference and (d) showing the vector control implementation.

Fig. 15 illustrates through the red dots the optimal excitation as well as stator d- and q-current components for a given operating torque. The constant torque lines are depicted by the blue dotted lines and the horizontal lines illustrate the d- and q-current references generating the lowest machine losses for a fixed excitation current as already shown in dotted lines on the 2D plot in Fig. 14. It can be seen that for low torque requirements, a low excitation current combined with a low d-current reference generates the smallest machine losses.

The result of the optimization shown in **Fig. 15**, is implemented as a lookup table for generating the d-current and the excitation current reference as shown in **Fig. 16** (c). The implementation of the SM control is shown in **Fig. 16**.

VI. RT-HIL EXPERIMENTAL RESULTS

Six scenarios are implemented on the RT-HIL platform:

- Run 1: $i_\mathrm{e}=8.8$ A, $i_\mathrm{d}=0$ A
- Run 2: $i_\mathrm{e}=8.8$ A, $i_\mathrm{d}=i_\mathrm{d}^{\mathrm{opt}}$
- Run 3: $i_\mathrm{e}=i_\mathrm{e}^{\mathrm{opt}}$, $i_\mathrm{d}=i_\mathrm{d}^{\mathrm{opt}}$
- Run 4: $i_\mathrm{e}=i_\mathrm{e}^{\mathrm{opt}}+0.5$ A, $i_\mathrm{d}=i_\mathrm{d}^{\mathrm{opt}}$
- Run 5: $i_\mathrm{e}=i_\mathrm{e}^{\mathrm{opt}}+1$ A, $i_\mathrm{d}=i_\mathrm{d}^{\mathrm{opt}}$
- Run 6: $i_\mathrm{e}=i_\mathrm{e}^{\mathrm{opt}}+1.5$ A, $i_\mathrm{d}=i_\mathrm{d}^{\mathrm{opt}}$

The here mentioned optimal values for the excitation and d-current correspond to the red line in **Fig. 15**, and are depending on the SM torque.

As the instantaneous power losses might not indicate accurately the differences among the various scenarios, the energy loss for a given time span will be used as a reference to determine the best scenario. In the case of the turbine start-up mode, as shown in Fig. 17, the total energy loss of the various runs is shown in table III. At the given operating conditions, the d-current reference takes relatively small values and thus has only a reduced impact on the overall losses as illustrated by comparing the first and second run. The impact of the excitation current however is significant considering the saving of up to 4.1%, especially considering the high amount of start-stop sequences that a flexible PHSP unit encounters throughout the day.

Similar observations can be done at full load operation, as illustrated on Fig. 18. While the small difference between no d-current and optimal d-current reference generates only a slight improvement considering the losses, the impact of the excitation current achieves more then 4.8% off loss reduction compared to the nominal operating conditions without optimization.

In both operating conditions presented in Fig. 17 and Fig. 18, the optimal system efficiency is achieved considering the optimal machine excitation current offset by 1 A. This offset is explained by the fact that the optimal machine operation does not include converter losses. The converter losses are reduced by reducing the overall current flowing through the branches. As this current is reduced by increasing the excitation current on the SM, it is expected that the optimal system efficiency is achieved by increasing the SM excitation current from its optimal value. This is validated in table IV, showing the average power losses of the different elements under full load operation.

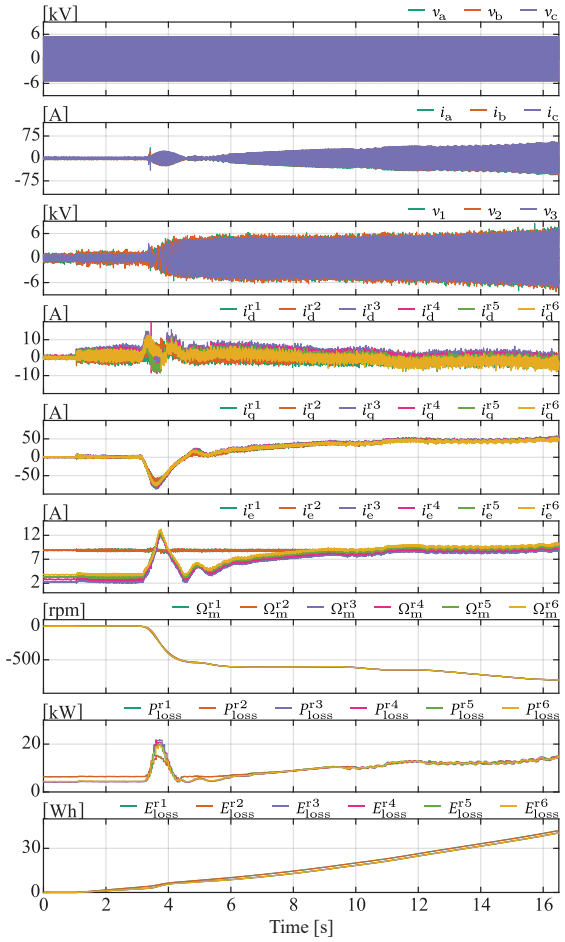

Fig. 17. HIL experimental results showing the various runs for the start in turbine mode. The speed and load torque profile correspond to the previously defined lowest damage trajectory. From top to bottom, the figure shows: grid voltages, grid currents, SM voltages, SM d-current, SM q-current, SM excitation current, SM speed, system power losses and system energy losses. The three phase plots are shown only for the first run.

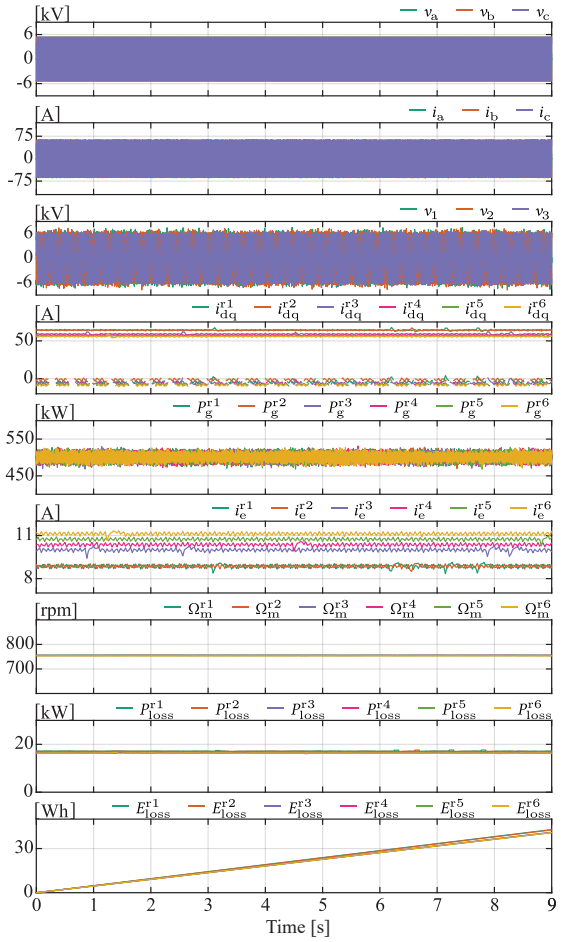

Fig. 18. HIL experimental results showing the various runs for the full load operation in pumping mode. From top to bottom, the figure shows: grid voltages, grid currents, SM voltages, SM d-current (dotted) and q-currents, M3C grid side terminal power, SM excitation current, SM speed, system power losses and system energy losses. The three phase plots are shown only for the first run.

TABLE III: Energy loss for the various runs.

Energy loss (Wh)	Machine start-up (after 16.5s)	Full load operation (after 9s)
Run 1	42.14 Wh	42.90 Wh
Run 2	41.99 Wh (-0.36%)	42.65 Wh (-0.58%)
Run 3	40.54 Wh (-3.80%)	41.09 Wh (-4.22%)
Run 4	40.47 Wh (-3.96%)	40.89 Wh (-4.68%)
Run 5	40.40 Wh (-4.13%)	40.82 Wh (-4.85%)
Run 6	40.47 Wh (-3.96%)	40.88 Wh (-4.71%)

TABLE IV: Average power losses under full load operation

	M3C	SM	Excitation	Total
Run 1	7.89 kW	9.23 kW	32 W	17.16 kW
Run 2	7.89 kW	9.15 kW	32 W	17.06 kW
Run 3	7.55 kW	8.85 kW	41 W	16.44 kW
Run 4	7.47 kW	8.85 kW	44 W	16.36 kW
Run 5	7.40 kW	8.89 kW	47 W	16.33 kW
Run 6	7.34 kW	8.96 kW	51 W	16.35 kW

VII. Conclusion

This paper presents a method for computing the M3C losses as well as the SM losses on a HIL platform as to enable a system loss optimization. Both these loss evaluations are done keeping the computational burden low as to allow implementation on the existing HIL platform used to validate the M3C control structure and algorithm. The here presented loss implementation runs on the RT Box 1, a small scale RT computer and enables for a loss computation at each simulation time-step of the RT simulator.

Complex converter topologies, such as M3C used in applications such as PHSP, rely on HIL simulations to validate the control structure and algorithm. Extending the HIL platform to include the system losses, allows for a fast optimization process for all possible operating points of the unit, including transients, as demonstrated in this paper.

As shown by the results presented in this work, the RT loss implementation allows for a low effort optimization of the drive and machine operating conditions. The reduced losses of up to 4.8%, as shown in the results, that can be achieved due to such optimization and considering the high amount of turbine starts throughout the day allow for both water and cost saving.

ACKNOWLEDGMENT

The results presented in this paper are a part of the Hydropower Extending Power System Flexibility (XFLEX HYDRO) project that has received funding from the European Union's Horizon 2020 research and innovation programme under grant agreement No 857832.

REFERENCES

[1] R. Grune, "Verlustoptimaler betrieb einer elektrisch erregten synchronmaschine für den einsatz in elektrofahrzeugen," 2013.

[2] F. Kammerer, D. Braeckle, M. Gommeringer, M. Schnarrenberger, and M. Braun, "Operating performance of the modular multilevel matrix converter in drive applications," in *Proceedings of PCIM Europe 2015; International Exhibition and Conference for Power Electronics, Intelligent Motion, Renewable Energy and Energy Management*, 2015, pp. 1–8.

[3] J. Kucka, D. Karwatzki, and A. Mertens, "Ac/ac modular multilevel converters in wind energy applications: Design considerations," in *2016 18th European Conference on Power Electronics and Applications (EPE'16 ECCE Europe)*, 2016, pp. 1–10.

[4] A. J. Korn, M. Winkelnkemper, P. Steimer, and J. W. Kolar, "Direct modular multi-level converter for gearless low-speed drives," in *Proceedings of the 2011 14th European Conference on Power Electronics and Applications*, 2011, pp. 1–7.

[5] W. Kawamura, K.-L. Chen, M. Hagiwara, and H. Akagi, "A low-speed, high-torque motor drive using a modular multilevel cascade converter based on triple-star bridge cells (mmcc-tsbc)," *IEEE Transactions on Industry Applications*, vol. 51, no. 5, pp. 3965–3974, 2015.

[6] M. Vasiladiotis, R. Baumann, C. Häderli, and J. Steinke, "Igct-based direct ac/ac modular multilevel converters for pumped hydro storage plants," in *2018 IEEE Energy Conversion Congress and Exposition (ECCE)*, 2018, pp. 4837–4844.

[7] A. Christe, A. Faulstich, M. Vasiladiotis, and P. Steinmann, "World's first fully rated direct ac/ac mmc for variable-speed pumped-storage hydropower plants," *IEEE Transactions on Industrial Electronics*, vol. 70, no. 7, pp. 6898–6907, 2023.

[8] S. Rohner, S. Bernet, M. Hiller, and R. Sommer, "Modulation, losses, and semiconductor requirements of modular multilevel converters," *IEEE Transactions on Industrial Electronics*, vol. 57, no. 8, pp. 2633–2642, 2010.

[9] M. Utvić, S. Milovanović, and D. Dujić, "Flexible medium voltage dc source utilizing series connected modular multilevel converters," in *2019 21st European Conference on Power Electronics and Applications (EPE '19 ECCE Europe)*, 2019, pp. 1–9.

[10] J. Freytes, F. Gruson, P. Delarue, F. Colas, and X. Guillaud, "Losses estimation method by simulation for the modular multilevel converter," in *2015 IEEE Electrical Power and Energy Conference (EPEC)*, 2015, pp. 332–338.

[11] S. Rodrigues, A. Papadopoulos, E. Kontos, T. Todorcevic, and P. Bauer, "Steady-state loss model of half-bridge modular multilevel converters," *IEEE Transactions on Industry Applications*, vol. 52, no. 3, pp. 2415–2425, 2016.

[12] A. Christe and D. Dujic, "Virtual submodule concept for fast semi-numerical modular multilevel converter loss estimation," *IEEE Transactions on Industrial Electronics*, vol. 64, no. 7, pp. 5286–5294, 2017.

[13] P. Bontemps, S. Milovanovic, and D. Dujic, "Distributed real-time model of the m3c for hil systems using small-scale simulators," *IEEE Open Journal of Power Electronics*, vol. 2, pp. 603–613, 2021.

[14] S. Milovanović, M. Luo, and D. Dujić, "Virtual capacitor concept for computationally efficient and flexible real-time mmc model," *IEEE Access*, vol. 9, pp. 144 211–144 226, 2021.

[15] D. Biner, S. Alligné, C. Nicolet, D. Dujic, and C. Münch-Alligné, "Numerical fatigue damage analysis of a variable speed francis pump-turbine during start-up in generating mode," in *IOP Conference Series: Earth and Environmental Science*, IOP Publishing, vol. 1079, 2022, p. 012 079.

[16] H. W. de Kock, A. J. Rix, and M. J. Kamper, "Optimal torque control of synchronous machines based on finite-element analysis," *IEEE Transactions on Industrial Electronics*, vol. 57, no. 1, pp. 413–419, 2010.

[17] Q. Wang, H.-H. Lee, H.-J. Park, S.-I. Kim, and G.-H. Lee, "An off-line maximum torque control strategy of wound rotor synchronous machine with nonlinear parameters," *Journal of Electrical Engineering and Technology*, vol. 11, no. 3, pp. 609–617, 2016.

[18] J. Reinhard, K. Löhe, and K. Graichen, "Optimal current setpoint computation for externally excited synchronous machines," in *2022 IEEE Conference on Control Technology and Applications (CCTA)*, 2022, pp. 1319–1326.

[19] J. Allmeling and N. Felderer, "Sub-cycle average models with integrated diodes for real-time simulation of power converters," in *2017 IEEE Southern Power Electronics Conference (SPEC)*, 2017, pp. 1–6.

[20] U. Nicolai and A. Wintrich, "Determining switching losses of semikron igbt modules," *SEMIKRON Application Note, AN*, vol. 1403, 2014.

[21] I. E. Commission *et al.*, "Rotating electrical machines–part 2-1: Standard methods for determining losses and efficiency from tests (excluding machines for traction vehicles)," IEC 60034-2-1, Tech. Rep., 2007.

[22] E. Levi, "Saturation modelling in d-q axis models of salient pole synchronous machines," *IEEE Transactions on Energy Conversion*, vol. 14, no. 1, pp. 44–50, 1999.

[23] A. Campeanu and M. Stiebler, "Modeling of saturation in salient pole synchronous machines," in *2010 12th International Conference on Optimization of Electrical and Electronic Equipment*, IEEE, 2010, pp. 258–263.

Philippe Bontemps received the B.Sc. and M.Sc. degrees from École Polytechnique Fédérale de Lausanne (EPFL), Lausanne, Switzerland, in 2017 and 2019, respectively. He is currently working towards the Ph.D. degree at École Polytechnique Fédérale de Lausanne (EPFL), Lausanne, Switzerland. In 2019, he joined Power Electronics Laboratory, EPFL, as a Doctoral Research Assistant. His research interests include multilevel conversion systems for high-power medium-voltage applications.

Daniel Biner obtained the B.Sc. and M.Sc. in Systems Engineering from the University of Applied Sciences and Arts Western Switzerland in 2014 and 2017, respectively. From 2017 to 2020 he worked as a full-time scientific assistant in the hydroelectricity research group of HES-SO Valais-Wallis. Since 2020 he is pursuing a doctoral work at EPFL-PEL, codirected by HES-SO Valais-Wallis. His main research interests include hydraulic and mechanical designs, field testing and numerical simulations of hydraulic turbomachinery.

Cécile Münch-Alligné obtained an engineering degree from INPG, Grenoble, France, in 2002. She received her doctoral degree on large eddy simulations of compressible turbulent flows in 2005 at the INPG. Since 2010, she has been Professor and head of the Hydroelectricity research team and the Hydro Alps at HES-SO Valais/Wallis, School of Engineering in Sion, Switzerland. Her main research interests are hydraulic turbomachinery, numerical simulations, performance measurements, turbulence and fluid-structure interactions.

Dražen Dujić received the Dipl. Ing. and M.Sc. degrees from the University of Novi Sad, Serbia, in 2002 and 2005, respectively, and the Ph.D. degree from Liverpool John Moores University, U.K., in 2008. He is an Associate Professor and the Head of the Power Electronics Laboratory at École Polytechnique Fédérale de Lausanne (EPFL), Lausanne, Switzerland. His research interests are predominantly related to high power conversion technologies for medium voltage applications.